Infinite Science Publishing

Proceedings Article

Magnetic particle imaging with non-oriented immobilized particles: Why the Langevin model of paramagnetism is sufficient

Marco Maass [a,b,*] · Christine Droigk [b] · Hannes Albers [c] · Konrad Scheffler [d,e] · Alfred Mertins [a,b] · Tobias Kluth [c] · Tobias Knopp [d,e]

[a] German Research Center for Artificial Intelligence (DFKI), Lübeck, Germany
[b] Institute for Signal Processing, University of Lübeck, Lübeck, Germany
[c] Center for Industrial Mathematics, University of Bremen, Bremen, Germany
[d] Section for Biomedical Imaging, University Medical Center Hamburg-Eppendorf, Hamburg, Germany
[e] Institute for Biomedical Imaging, Hamburg University of Technology, Hamburg, Germany
*Corresponding author, email: marco.maass@dfki.de

Abstract

The Langevin model of paramagnetism is commonly used as a simplified physical model for magnetic particle imaging. In research with immobilized nanoparticles that are non-oriented, the phenomenon is observed that the measured system function components for Lissajous trajectory-based excitation show a high spatial similarity to those from the Langevin model of paramagnetism. In this work we show that this observation can be explained mathematically, since in equilibrium and for anisotropic uniaxial nanoparticles without orientation the model falls back to the Langevin model of paramagnetism. Since previous studies have also shown that the anisotropic equilibrium model for immobilized particles is approximately equivalent to the Néel rotation Fokker-Planck model, the Langevin model of paramagnetism is sufficient to cover the non-oriented immobilized case.

I. Introduction

For model-based magnetic particle imaging (MPI), it is of utmost importance to have good physical models for the magnetic moment of superparamagnetic nanoparticles (SPIOs). In a first attempt, the Langevin model of paramagnetism has been used, which allows for fast simulation of the MPI systems [1]. However, the model is rather simplified as it neglects particle anisotropies and magnetization dynamics. If anisotropies of the particles are taken into account, the Stoner-Wolfarth model is usually used to model the magnetic moment of the nanoparticles with a uniaxial anisotropy [2]. Since the Stoner-Wolfarth model is very simple, typical SPIOs show a more com-

plex anisotropy that cannot be properly explained by the Stoner-Wolfarth model [3]. The magnetization mechanisms are usually described by the Néel rotation, which describes the internal rotation of the magnetic moment, and the Brownian rotation, which describes the spatial rotation of the entire particle. Various models and methods can be used to simulate the coupled dynamics [4, 5]. Although these models allow for a better explanation of the imaging process, they have the disadvantage that the simulation is time-consuming. As an intermediate solution, it has been investigated whether it is possible for typical SPIO distributions and MPI scanners to replace the probability density function, which is obtained by numerically solving a Fokker-Planck equation (FP), with

an equilibrium (EQ) model with anisotropy (EQA) [6–8]. In order to neglect Brownian rotation, the behavior of immobilized particles with oriented [7, 9] and non-oriented [10] SPIOs was investigated. The parameter identification of the FP model in [10] leads to a model with a small anisotropy constant. In this work, we show that this does not happen by chance because if the SPIO distribution is perfectly non-oriented and immobilized, i.e., the anisotropy directions are uniformly distributed, the EQA model becomes an EQ model without anisotropy. In addition, for a typical SPIO tracer and a Lissajous-type MPI sequence, the Néel rotation FP model [11, B1] and the EQA model are very close to each other [9]. Furthermore, the theoretical findings in this article are analyzed on the basis of system function components (SFCs) using simulated as well as experimental data.

II. Methods and Materials

The assumption is made that the monodisperse particles are modeled with the same particle diameter, the same anisotropy constant and a uniaxial easy axis, and that the particles have been immobilized so that Néel rotation is the only magnetization mechanism. The mean magnetic moment can be derived from the partition function (PF) by

$$\bar{\boldsymbol{m}}(\boldsymbol{H};\mathbb{O}) = \frac{m_0}{\beta} \nabla_H \ln(\mathcal{Z}(\boldsymbol{H},\mathbb{O})) = \frac{m_0}{\beta} \frac{\nabla_H \mathcal{Z}(\boldsymbol{H},\mathbb{O})}{\mathcal{Z}(\boldsymbol{H},\mathbb{O})}.$$

and is given for immobilized and oriented SPIOs in the thermodynamical EQ with the easy axis $\boldsymbol{n} \in \mathbb{S}^2$ by

$$\mathcal{Z}(\boldsymbol{H};\mathbb{O}) = \int_{\mathbb{S}^2} e^{\beta H^T m + \alpha_K (n^T m)^2} \, d\boldsymbol{m},$$

where $\mathbb{O} = \{\alpha_K, \boldsymbol{n}\}$ denotes the observable parameter set in the Boltzmann distribution, α_K an anisotropy strength, $\boldsymbol{H} \in \mathbb{R}^3$ the applied magnetic field, $\beta > 0$ a physical parameter dependent on the particle diameter, and the argument parameter $\boldsymbol{m} \in \mathbb{S}^2$. Besides, m_0 denotes the magnitude of the magnetic moment of one SPIO. Note that $\mathbb{S}^2$ denotes the surface of the unit sphere.

However, what if the SPIO are immobilized but the easy axes of the SPIOs are uniformly distributed? Based on the Néel rotation FP model, such a situation was investigated in [10] for a polydisperse model. The analysis of the results in the previous article showed that the anisotropy constant α_K was estimated rather small.

In the following, it is shown that for the investigated case, the EQA model leads to an EQ model without anisotropy. To show this, the PF is examined and a uniformly distributed easy axis $\boldsymbol{n} \sim \mathcal{U}(\mathbb{S}^2)$ is assumed. The structural concept of the following derivations was adopted from [12, Appendix]. Hence, the following applies

$$\mathcal{Z}(\boldsymbol{H};\underbrace{\{\alpha_K, \boldsymbol{n} \sim \mathcal{U}(\mathbb{S}^2)\}}_{=\tilde{\mathbb{O}}}) = \int_{\mathbb{S}^2} \int_{\mathbb{S}^2} e^{\beta H^T m + \alpha_K (n^T m)^2} \, d\boldsymbol{m} \, d\boldsymbol{n}$$

$$= \int_{\mathbb{S}^2} e^{\beta H^T m} \underbrace{\int_{\mathbb{S}^2} e^{\alpha_K (n^T m)^2} \, d\boldsymbol{n}}_{=\mathcal{R}(\alpha_K, \boldsymbol{m})} \, d\boldsymbol{m},$$

where the change in the order of integration is allowed because the function $e^{\beta H^T m + \alpha_K (n^T m)^2}$ is continuous for all $\boldsymbol{n}, \boldsymbol{m} \in \mathbb{S}^2$, therefore the Fubini theorem can be applied. The inner integral $\mathcal{R}(\alpha_K, \boldsymbol{m})$ is to be investigated. First, choose a rotation matrix $\boldsymbol{R}_m \in \mathbb{R}^{3 \times 3}$ such that $\boldsymbol{e}_3 = \boldsymbol{R}_m \boldsymbol{m}$, where $\boldsymbol{e}_3$ is the third Euclidean unit vector and perform the substitution $\tilde{\boldsymbol{n}} = \boldsymbol{R}_m \boldsymbol{n}$ in the integral. Due to $\boldsymbol{R}_m$ being orthogonal, $\boldsymbol{R}_m^T \boldsymbol{R}_m = \boldsymbol{I}$, where $\boldsymbol{I} \in \mathbb{R}^{3 \times 3}$ is the unit matrix, and $|\det(\boldsymbol{R}_m)| = 1$. Thus, we get $d\tilde{\boldsymbol{n}} = |\det(\boldsymbol{R}_m)| d\boldsymbol{n} = d\boldsymbol{n}$ and therefore the following applies

$$\mathcal{R}(\alpha_K, \boldsymbol{m}) = \int_{\mathbb{S}^2} e^{\alpha_K (n^T R_m^T R_m m)^2} \, d\boldsymbol{n} = \int_{\mathbb{S}^2} e^{\alpha_K \tilde{n}_3^2} \, d\tilde{\boldsymbol{n}}.$$

Using spherical coordinates $(\tilde{n}_1 = \sin(\vartheta)\cos(\varphi), \tilde{n}_2 = \sin(\vartheta)\sin(\varphi), \tilde{n}_3 = \cos(\vartheta), \vartheta \in [0, \pi], \varphi \in [0, 2\pi])$ followed by the substitution $x = \cos(\vartheta)$ one obtains

$$\mathcal{R}(\alpha_K, \boldsymbol{m}) = F(\alpha_K) = 2\pi \int_{-1}^{1} e^{\alpha_K x^2} \, dx.$$

The function $\mathcal{R}(\alpha_K, \boldsymbol{m})$ is constant in $\boldsymbol{m}$ and can be expressed as a function $F(\alpha_K)$ independent of $\boldsymbol{m}$. Therefore, the PF is

$$\mathcal{Z}(\boldsymbol{H};\tilde{\mathbb{O}}) = F(\alpha_K) \int_{\mathbb{S}^2} e^{\beta H^T m} \, d\boldsymbol{m} = 4\pi F(\alpha_K) \frac{\sinh(\beta \|\boldsymbol{H}\|)}{\beta \|\boldsymbol{H}\|}.$$

Since α_K is independent of $\boldsymbol{H}$ and because the mean magnetic moment can be derived from the PF, we obtain

$$\bar{\boldsymbol{m}}(\boldsymbol{H};\tilde{\mathbb{O}}) = \frac{m_0}{\beta} \nabla_H \ln(\mathcal{Z}(\boldsymbol{H},\tilde{\mathbb{O}})) = m_0 \mathscr{L}(\beta \|\boldsymbol{H}\|_2) \frac{\boldsymbol{H}}{\|\boldsymbol{H}\|_2},$$

with $\mathscr{L}(\xi)$ being the Langevin function. Thus, for immobilized non-oriented particles, the EQA model is equivalent to the Langevin model of paramagnetism.

II.I. Experiment

It should be checked numerically whether the Langevin model of paramagnetism is good enough to describe the Néel rotation FP model and a measured system function when the SPIOs are immobilized and non-oriented. Therefore, a 2D system matrix with spatial discretization of 17×15 is measured with a delta sample of size $2 \times 2 \times 2$ cm^3 filled with perimag at a concentration of $10 \, \text{mol}_{FE}/\text{l}$. Bruker's preclinical MPI scanner is used with
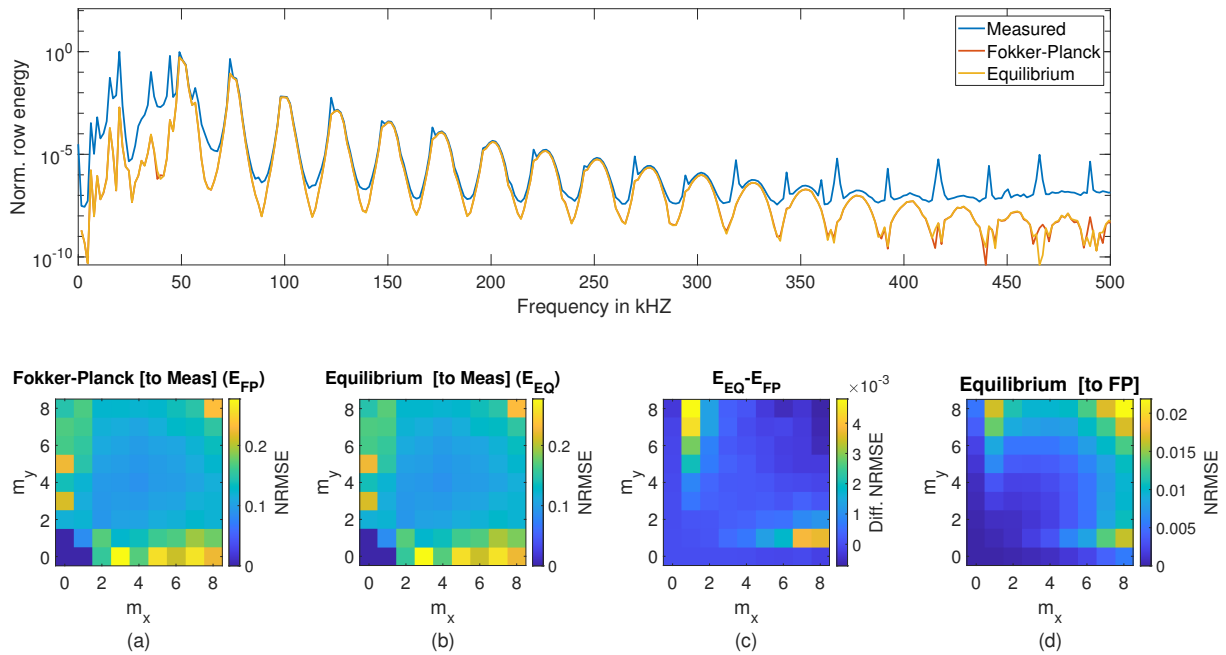
Figure 1: The top row shows the row energy of the SFCs as a function of the frequency. The bottom row shows different error measures depending on the mixing orders m_x and m_y. The bottom row shows from left to right the NRMSE of the FP-SFC to the measured SFC (a), the EQ-SFC to the measured SFC (b), the difference between the NRMSEs of the two left diagrams (c), and the NRMSE between EQ-SFC and FP-SFC (d).

a gradient strength of $(-1, -1, 2)\,\text{T}\,\text{m}^{-1}$ and a cosine drive-field excitation with a frequency ratio of $f_x/f_y = 16/17$ ($f_x = 2.5/102$ MHz) and amplitudes of $(0.012, 0.012, 0)$ T. The FP simulation for the Neél rotation is carried out using the toolbox of [13]. The EQ model is simulated using the Langevin function. The optimal particle diameter was found to be 22 nm for both models. The transfer function is determined using the least squares method according to [14]. The normalized root means square error (NRMSE) is calculated by the measure in [9]. For the comparison, mixing orders are used that assign the temporal frequency index $k \in \mathbb{Z}$ to the spatial frequency orders $m_x, m_y \in \mathbb{Z}$, where the following applies: $k = 16 m_x + 17 m_y$.

III. Results

The top row in Figure 1 shows the row energy of the measured SFCs, FP-SFCs, and EQ-SFCs [15]. The energy is normalized so that the largest energy value of the measured SFC is normalized to 1. It can be seen that different SFCs between 75 kHz and 360 kHz, that have high energy, match quite well. For low energy SFCs, a slightly lower energy can be observed in the model-based SFCs. For model-based FP-SFCs and EQ-SFCs no substantial differences are visually apparent. The two Figures 1 (a)

and (b) show the NRMSE of the model-based SFCs to the measured SFCs as function of the mixing orders. The mixing orders $(0, 0)\,(0, 1)\,(1, 0)$ are removed, as no or only a very low SPIO signal is expected due to the filtering in the receive chain. A relatively high error is observed near the zero mixing order, which could be due to the harmonics of the drive field sequences and the filtering to remove these harmonics from the measured signal. After zero mixing orders, the NRMSE decreases sharply and then increases slightly with increasing mixing order. The two Figures 1 (c) and (d) show that the two SFC models do not differ significantly from each other. As can be seen in Figure 1 (c), the NRMSE difference between two models is in the range $-0.7 \cdot 10^{-3}$ and $4.7 \cdot 10^{-3}$. For small mixing orders, the FP model has the smaller NRMSE, but for larger mixing orders with $m_x \geq 5$ and $m_x \geq 5$ the EQ model has a smaller error, which might depend on the numerical solution of the FP equations. The difference in the NRMSE is two orders of magnitude smaller than the NRMSE in Figures 1 (a) and (b), which indicates a very small difference between the two models in terms of modeling quality. The comparison of the EQ model with the FP model in Figure 1 (d) shows that the NRMSE for $|m_y|, |m_x| \leq 8$ is relatively small with a maximum value of about 0.02 and that the NRMSE increases with increasing mixing order.

IV. Discussion and Conclusion

For the EQ model with anisotropy the mathematical proof shows that the influence of SPIO anisotropy is eliminated if the SPIOs are immobilized and non-oriented, i.e., have uniformly distributed easy axis. Although the FP model behaves similarly as observed in the results in [10] and [11, Fig. 2], it is not entirely clear whether a similar result can be derived for the FP case, i.e. that the non-oriented FP model is equivalent to the FP model [11, B1]. However, the numerical results show that the influence of anisotropy is small in the non-oriented case. It should be mentioned that the particle model with immobilized and non-oriented SPIOs investigated here is a rather specialized scenario for MPI, suitable, for example, for tracking medical instruments such as stents. In contrast, in a more realistic scenario, where the SPIOs are immobilized to a certain degree, one would expect Brownian rotation to rotate the SPIOs towards their local energetic optimum, i.e. in this model, for example, towards the uniaxial easy axis. One would thus observe a kind of commutative anisotropy effect that depends on the strength of the magnetic field and the degree of immobilization. Nevertheless, the theoretical and practical insight that the Langevin model of paramagnetism itself is sufficient for this particle model has its own value.

Author's statement

Conflict of interest: Authors state no conflict of interest.

References

[1] J. Weizenecker, J. Borgert, and B. Gleich. A simulation study on the resolution and sensitivity of magnetic particle imaging. *Phys. Med. Biol.*, 52(21):6363–6374, 2007, doi:10.1088/0031-9155/52/21/001.

[2] E. C. Stoner and E. P. Wohlfarth. A mechanism of magnetic hysteresis in heterogeneous alloys. *Philos. Trans. R. Soc. A*, 240(826):599–642, 1948, doi:10.1098/rsta.1948.0007.

[3] A. Neumann and T. M. Buzug. Simulations of magnetic particles with arbitrary anisotropies. *Int. J. Magn. Part. Imaging*, 6(2 Suppl 1), 2020, doi:10.18416/IJMPI.2020.2009032.

[4] M. Graeser, K. Bente, A. Neumann, and T. M. Buzug. Trajectory dependent particle response for anisotropic mono domain particles in magnetic particle imaging. *J. Phys. D: Appl. Phys.*, 49(4):045007, 2015, doi:10.1088/0022-3727/49/4/045007.

[5] J. Weizenecker. The Fokker–Planck equation for coupled Brown–Néel-rotation. *Phys. Med. Biol.*, 63(4):035004, 2018, doi:10.1088/1361-6560/aaa186.

[6] M. Maass, C. Droigk, M. Eulers, and A. Mertins. An analytical equilibrium solution to the Néel relaxation Fokker-Planck equation. *Int. J. Magn. Part. Imaging*, 8(1 Suppl 1), 2022, doi:10.18416/IJMPI.2022.2203008.

[7] H. Albers and T. Kluth. Immobilized nanoparticles with uniaxial anisotropy in multi-dimensional Lissajous-type excitation: An equilibrium model approach. *Int. J. Magn. Part. Imaging*, 8(1 Suppl 1), 2022, doi:10.18416/IJMPI.2022.2203048.

[8] M. Maass, C. Droigk, M. Eulers, and A. Mertins. A system function component model for magnetic particle imaging with anisotropic particles. *Int. J. Magn. Part. Imaging*, 9(1 Suppl 1), 2023, doi:10.18416/IJMPI.2023.2303076.

[9] H. Albers, T. Knopp, M. Möddel, M. Boberg, and T. Kluth. Modeling the magnetization dynamics for large ensembles of immobilized magnetic nanoparticles in multi-dimensional magnetic particle imaging. *J. Magn. Magn. Mater.*, 543:168534, 2022, doi:10.1016/j.jmmm.2021.168534.

[10] H. Albers, F. Thieben, M. Boberg, K. Scheffler, T. Knopp, and T. Kluth. Model-based calibration and image reconstruction with immobilized nanoparticles. *Int. J. Magn. Part. Imaging*, 9(1 Suppl 1), 2023, doi:10.18416/IJMPI.2023.2303002.

[11] T. Kluth, P. Szwargulski, and T. Knopp. Towards accurate modeling of the multidimensional magnetic particle imaging physics. *New J. Phys.*, 21(10):103032, 2019, doi:10.1088/1367-2630/ab4938.

[12] K. Morozov, M. Shliomis, and M. Zahn. Magnetoviscosity in suspensions of grains with finite magnetic anisotropy. *Phys. Rev. E*, 73:066312, 6 2006, doi:10.1103/PhysRevE.73.066312.

[13] H. Albers, T. Kluth, and T. Knopp. Simulating magnetization dynamics of large ensembles of single domain nanoparticles: Numerical study of Brown/Néel dynamics and parameter identification problems in magnetic particle imaging. *J. Magn. Magn. Mater.*, 541:168508, 2022, doi:10.1016/j.jmmm.2021.168508.

[14] T. Knopp, S. Biederer, T. F. Sattel, J. Rahmer, J. Weizenecker, B. Gleich, J. Borgert, and T. M. Buzug. 2D model-based reconstruction for magnetic particle imaging. *Med. Phys.*, 37(2):485–491, doi:10.1118/1.3271258.

[15] T. Knopp, J. Rahmer, T. F. Sattel, S. Biederer, J. Weizenecker, B. Gleich, J. Borgert, and T. M. Buzug. Weighted iterative reconstruction for magnetic particle imaging. *Phys. Med. Biol.*, 55(6):1577, 2010, doi:10.1088/0031-9155/55/6/003.